*International Journal of Automotive Technology*, Vol. 8, No. 3, pp. 309–317 (2007)


1229-9138/2007/034-07

# OPTIMAL SHAPE DESIGN OF THE FRONT WHEEL LOWER CONTROL ARM CONSIDERING DYNAMIC EFFECTS

B. J. KANG*, H.-C. SIN and J. H. KIM

School of Mechanical and Aerospace Engineering, Seoul National University, Seoul 151-744, Korea

*(Received 17 November 2006; Revised 22 April 2007)*

**ABSTRACT**–In this study, we conducted a vibration fatigue analysis of the lower control arm in a vehicle suspension system. The vehicle was driven during the tests so that the dynamic effects could be taken into account. The dynamic load of the frequency domain was superimposed on the frequency response analysis. We performed a virtual proving ground test using multi-body dynamics, along with a finite element analysis and fatigue life predictions. Shape optimization was also considered using the design of the experimental approach, and a response surface analysis was performed to improve the durability performance of the lower control arm. We identified the elements that had the most influence on the optimal shape of the finite element model and analyzed the sensitivity of those elements. Then the optimal points that minimized the amount of damage to the areas of interest were determined through a response surface analysis. The results suggested that the fatigue life of the model increased as its mass was not increased excessively, and demonstrated that these design procedures yielded an appropriate optimized lower control arm model.

**KEY WORDS :** Vibration fatigue analysis, Response surface analysis, Vehicle dynamic analysis, Frequency response analysis, Orthogonal array table, Suspension system

## 1. INTRODUCTION

The fatigue life of a structure is generally predicted in the final stages of the design process since the stress and strain profiles required for the analysis can be obtained from a prototype. A durability analysis can be easily mistaken as the only procedure used to confirm whether a designed model is adequate. Accurate predictions of the fatigue life are as important as other design procedures since they permit the designer to reduce the amount of materials and cut other structural costs.

Accurate predictions of the fatigue life of various parts of a vehicle are very important when it comes to the overall vehicle design. The designer performs a durability analysis of each part in the early stages of the design. Driving tests on a durability test road and road simulators allow the designer to obtain load profiles upon which the durability analysis is based using finite element models of each part (Bishop *et al.*, 2000; Haiba *et al.*, 2003). Durability analyses are also performed using simulations based on a virtual proving ground test approach, which takes into account the cost and time invested (Kim *et al.*, 2002). Considerable efforts have been made to optimize the models to improve the durability performance in terms of the reliability of the design (Choi *et al.*, 2005a, 2005b).

In a vibration fatigue analysis, the dynamic load in the time domain obtained through a conventional driving test is first converted into the frequency domain using a fast Fourier transformation. It is then superimposed upon the outcome of a frequency response analysis to obtain the durability life of a structure (Dirlik, 1985; Bishop and Sheratt, 1989). This approach yields a more accurate evaluation of the durability life since it considers excitations that occur in the structure up to its natural frequency. Thus, a vibration fatigue analysis is suitable for structures that are sensitive to vibrations, including suspension system parts such as the lower control arm (Lee *et al.*, 2003; Jung and Bae, 2005).

In this study, we calculated the dynamic load obtained during a Belgian road virtual proving ground test using ADAMS (1998), a commercial code for sport utility vehicles (SUVs). We confirmed that resonance occurred while driving on Belgian roads based on a mode and frequency response analysis of the lower control arm. We performed a vibration fatigue analysis to evaluate the durability life of the lower control arm and optimized the shape of the arm using the design of the experiment and response surface approaches. We then proposed a model to improve the durability life of the lower control arm while maintaining its weight. MSC/NASTRAN (2002) was used to obtain the mode and frequency response,

*Corresponding author. e-mail: mechania@hotmail.com

while MSC/FATIGUE (2003) was used for the durability analysis.

## 2. VIBRATION FATIGUE ANALYSIS

### 2.1. Theoretical Background

In general, one can use either a quasi-static fatigue approach or a vibrational fatigue approach to perform a durability analysis. A quasi-static fatigue analysis evaluates the fatigue life by combining the results of a static structural analysis with those of a calculated dynamic load profile. Thus, the approach is valid when the structure is not subjected to the dynamic behavior effects. A vibration fatigue analysis includes the dynamic effects of the structure. Unlike a conventional S-N approach, however, it requires the power spectral density of the frequency domain of the load profile along with the outcome of the frequency response analysis of the subject model (Bishop and Sheratt, 1989). It converts the dynamic load from the time domain to the frequency domain using a fast Fourier transformation and calculates the stress distribution as a function of frequency using a power spectral density function. If the input is in the format of a power spectral density, the output will also be in the format of a power spectral density, making it impossible to calculate the fatigue life. Thus, the spectral moment must be calculated from the power spectral density and then converted into a probability density function, from which the fatigue life can be computed.

### 2.2. Fatigue Analysis Approach for Damage Rates

In a vibration fatigue analysis, the damage rate, $D$, can be represented using a modified form of the conventional Miner's rule (Lee *et al.*, 2005):

$$D = \sum_{i=1}^{k} \frac{n_i}{N_{f,i}} \tag{1}$$

where $n_i$ is the total number of cycles in the $i^{th}$ block of the constant-stress amplitude $S_{a,I}$, $N_{f,I}$ is the number of cycles to failure under $S_{a,I}$, and $k$ is the total number of blocks. Failure occurs when $D \geq 1$.

Bendat (1964) assumed that all the peaks of a narrow-band random process have counter-peaks of the same height, since the probability density function of such peaks has a Rayleigh distribution. Based on this assumption, he suggested an approach to calculate the fatigue life from the stress power spectral density. This approach, however, tends to predict a fatigue life that is too short when applied to a wideband random process.

The damage rate proposed by Dirlik (1985) for a fatigue analysis of a wideband random process is:

$$D_{WB,Dirlik} = \frac{E[P]\tau}{b} \int_0^{\infty} S_a^m \, fs_a(S_a) dS_a \tag{2}$$

where $E[P]$ refers to the expectation value of the peak, while $S_a$ is the constant-stress amplitude on the entire block, $fs_a(S_a)$ is the probability density function for the stress amplitude $S_a$, and $b$ and $m$ are the intercept and slope of the measured S-N plot. The corresponding probability density function $fs_a(S_a)$ can be obtained using a Monte Carlo technique and assuming that $fs_a(S_a)$ has an impact on the fatigue life of a wideband random process analysis:

$$fs_a(S_a) = \frac{D_1}{2\sqrt{M_0}Q} e^{\frac{-Z}{Q} \times s_a} + \frac{D_2 \times Z}{2\sqrt{M_0}R^2} e^{\frac{-Z^2}{2R^2} \times s_a^2} + \frac{D_3 \times Z}{2\sqrt{M_0}} e^{\frac{-Z^2}{2} \times s_a^2} \tag{3}$$

$$Z = \frac{1}{2\sqrt{M_0}}, \quad \gamma = \frac{M_2}{\sqrt{M_0 M_4}}, \quad X_m = \frac{M_1}{M_0}\sqrt{\frac{M_2}{M_4}} \tag{4}$$

$$D_1 = \frac{2(X_m - \gamma^2)}{1+\gamma^2}, \; D_2 = \frac{1-\gamma-D_1+D_1^2}{1-R}, \; D_3 = 1 - D_1 - D_2 \tag{5}$$

$$R = \frac{\gamma - X_m - D_1^2}{1-\gamma-D_1+D_1^2} \tag{6}$$

$$Q = \frac{1.25(\gamma - D_3 - D_2 \times R)}{D_1} \tag{7}$$

where $D_1$, $D_2$, $D_3$, and $R$ are all functions of $M_0$, $M_1$, $M_2$, and $M_4$, respectively, and $Z$ is a normalized variable.

The probability density function $fs_a(S_a)$, given above is represented by a complicated formula but can be calculated from the four factors $M_0$, $M_1$, $M_2$, and $M_4$, which are area moments obtained from the stress power spectral density. These four factors represent the specific values of the area, and the average and distribution of the power spectral density.

Based on Dirlik's empirical closed-form expression, Bishop (1988) proposed a theoretical formula to predict the range of the rainflow out of the area moment of the power spectral density. However, Dirlik's approach is more widely used for vibration fatigue analyses, since it is easier to calculate and generates better results.

## 3. VEHICLE ANALYSIS MODEL

### 3.1. Multibody Dynamic Model for a Virtual Ground Proving Test

A virtual proving ground test performed to calculate the dynamic load applied to the parts of the suspension. A four-wheel drive SUV was used with front wheel McPherson struts and a rear wheel double wishbone suspension system. The entire vehicle model is depicted in Figure 1, and its components are listed in Table 1. A commercial program, ADAMS/View, was used to model the suspension and perform the virtual proving ground test. The vehicle model properties are listed in Table 2.

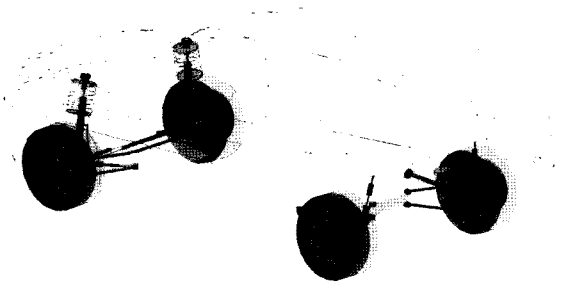

Figure 1. Vehicle dynamic model for the the virtual proving ground test.

Table 1. Components of the vehicle model.

| Component | Number |
|---|---|
| Moving parts | 63 |
| Cylindrical joints | 2 |
| Revolute joints | 7 |
| Spherical joints | 10 |
| Translational joints | 3 |
| Fixed joints | 33 |
| Hooke joints | 4 |
| Motions | 7 |
| Degree of freedom | 69 |

Table 2. Vehicle model properties.

| | |
|---|---|
| Component mass | |
| Gross vehicle (kg) | 2068 |
| Chassis (kg) | 1851 |
| Moment of inertia of the chassis | |
| Roll moment of inertia (kg mm$^2$) | 507.29E-6 |
| Pitch moment of inertia (kg mm$^2$) | 3501.11E-6 |
| Yaw moment of inertia (kg mm$^2$) | 3805.30E-6 |
| Front suspension | |
| Spring stiffness (N/mm) | 27 |
| Damping rate | Figure 2 (a) |
| Rear suspension | |
| Spring stiffness (N/mm) | 51 |
| Damping rate | Figure 2 (b) |
| Stabilizer bar (N mm/deg) | 40344 |
| Tire | |
| Radius (mm) | 336 |
| Vertical stiffness (N/m) | 170 |
| Lateral stiffness (N/m) | 50 |
| Cornering stiffness (N/m) | 69.87 |

The kinetic behavior of the suspension was considered to compute the loading encountered during the virtual proving ground events in the attachment elements of the chassis. Since the body was a fully developed product, it contained sufficient stiffness to cause deformation, which affected its handling performance. Thus, the body model was assumed to be completely rigid in vehicle simulations at a relatively slow speed of 20 km/h (Heinrietz *et al.*, 2003; Berzri *et al.*, 2004; Ghosh and Medepalli, 2005).

The front wheel suspension system included the lower control arms, knuckles, shock absorber assembly, and a subframe. These components were connected to each other with a variety of attachment elements, such as bushings and joints.

The knuckle is joined rigidly to the strut and connected to the lower control arm with a spherical joint to form a ball joint. In the model of the force elements, the spring element is approximated as being linear, and the damper elements which are embodied in spline curves that were obtained from a characteristic test of the damper were

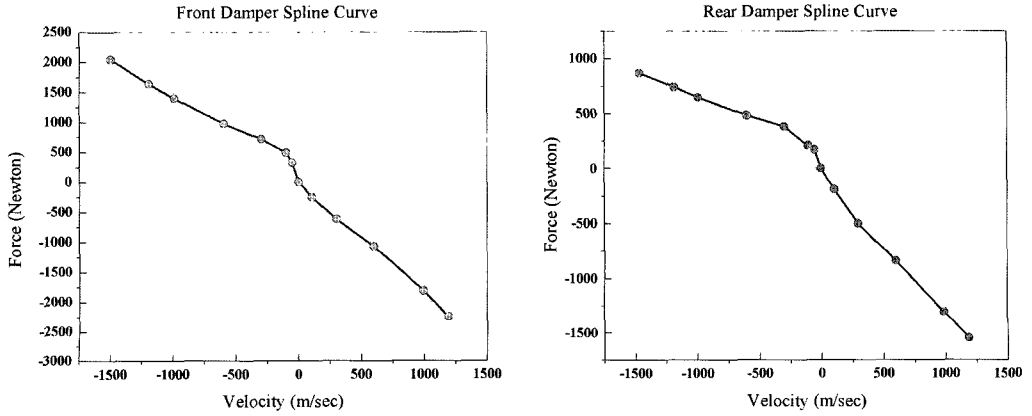


(a) Front damper spline curve (b) Rear damper spline curve

Figure 2. Nonlinear damper properties.

used to consider the nonlinear behavior; the tire is the modeled part with shape, mass and stiffness as prototype. Figure 2 shows the damper properties.

The input data required for the dynamic load analysis included wheel loads measured simultaneously on the four wheels while driving. However, the driving test is normally performed by attaching a wheel tranceducer either to the front or rear wheel. Therefore, in this study, in order to obtain the load profile in the front wheel, six axis loads on the right and left front wheels were entered into the system to obtain the dynamic loads for the durability analysis. Vertical displacement values obtained by integrating the acceleration signals twice were used for the rear wheels. The forces obtained at the front wheel parts, such as the ball joint, spring, damper, tie rod end, and stabilizer bar link, were analyzed. In addition, as the vehicle model could be unstable in cases of the wheel loads being imposed without constraints of the vehicle model in the boundary condition (Kim *et al.*, 2003), vehicle bouncing, pitch and roll were only considered by restraining translational motion in the x and y axies, and rotational motion in the z axis of the mass center of the body model considering x, y directional motion and yaw being small in the virtual driving test. Figure 3 depicts the

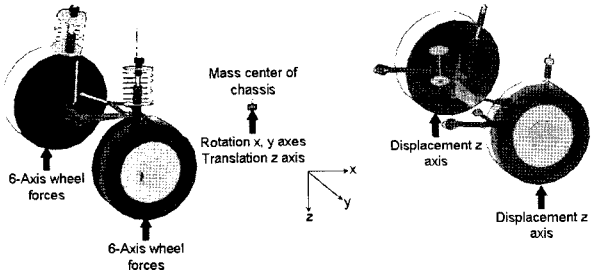


Figure 3. Load and displacement input for computing the dynamic load.

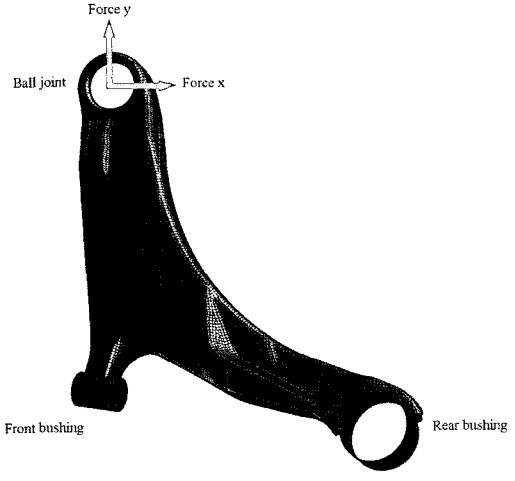


Figure 4. Finite element model of the lower control arm.

Table 3. Lower control arm properties.

| FE model information | |
|---|---|
| Node | 16811 |
| Shell element | 17084 |
| **Properties** | |
| Young's modulus (Mpa) | 2.1E5 |
| Poisson's ratio | 0.3 |
| Density (kg/mm$^3$) | 7.9E-6 |
| Yield strength (Mpa) | 410 |
| Ultimate tensile strength (Mpa) | 550 |
| Mass (kg) | 3.62 |

load input and displacement conditions for the virtual proving ground test.

### 3.2. Finite Element Model of the Lower Control Arm

The finite element model shown in Figure 4 was used to conduct the durability analysis of the lower control arm.

Since the lower control arm was made of a thin plate, it was modeled using shell elements. The front and rear bushings were joined to the subframe and a ball joint connected the knuckle. Since the lower control arm was connected to the cross member with two bushing elements, the point at which they were joined was fixed as the center and the analysis loads were imposed at the ball joint. The force analysis loads were therefore the loads of the $x$- and $y$-axes of the ball joint. The material properties of the finite elements used for the analysis are listed in Table 3.

## 4. VIBRATION FATIGUE ANALYSIS

### 4.1. Process

A vibration fatigue analysis that considers dynamic effects is not much different from a fatigue analysis performed in the time domain, except that we work in the frequency domain and require a fatigue modeler to transform the

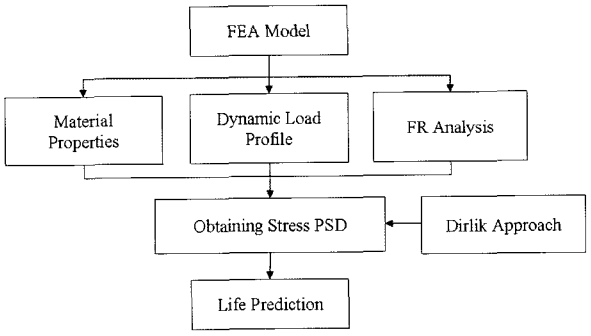


Figure 5. Schematic diagram of the vibration fatigue analysis.

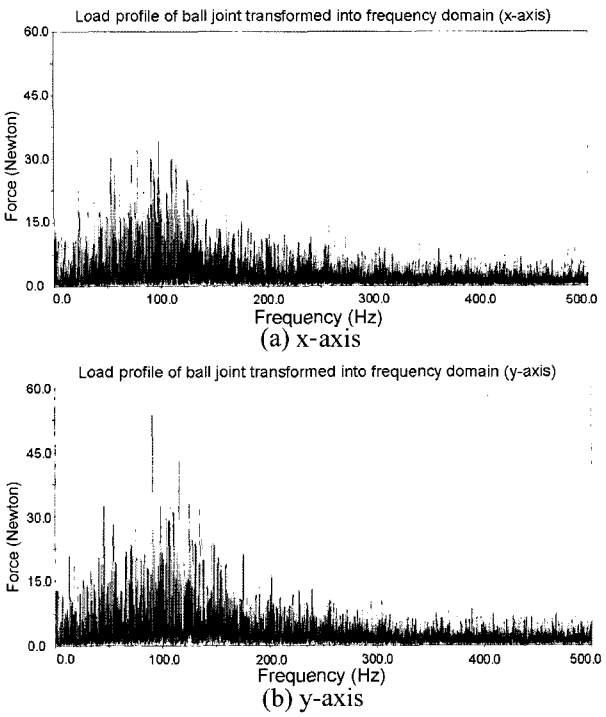


Figure 6. Dynamic load profile of the ball joint transformed into the frequency domain.

stress power spectral density to the rainflow cycle histogram. The vibration fatigue analysis procedure is illustrated in Figure 5.

4.2. Calculation of the Dynamic Load in the Frequency Domain

The dynamic loads of the $x$- and $y$-axes of the ball joint in the frequency domain can be obtained using a fast Fourier transformation of the dynamic loads in the time domain calculated from the virtual proving ground test. These are shown in Figure 6, which indicates that the lower control arm was excited up to 500 Hz while driving on the Belgian roads. The mode analysis showed that the natural frequency of the lower control arm was 294 Hz, which is within the range of excitation. Therefore, dynamic effects cannot be ignored in the durability analysis. It is desirable to evaluate the durability life of the lower control arm using a vibration fatigue analysis. Figure 7 shows the primary natural frequencies obtained through the mode analysis.

4.3. Frequency Response and Vibration Fatigue Analysis

A frequency response analysis was performed at 2-Hz intervals from 0 to 500 Hz. A unit load was applied in the $x$- and $y$-directions at the ball joint. The maximum stress occurred at node 945, which was located on the curve under the front bushing. Figure 8 shows the outcome of

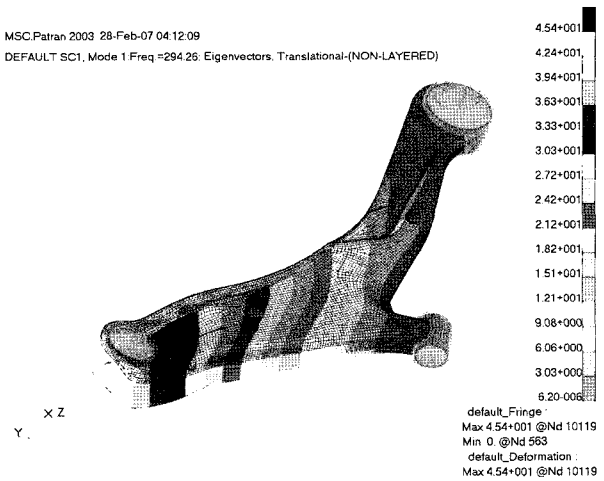


Figure 7. Primary vibrational mode of the lower control arm.

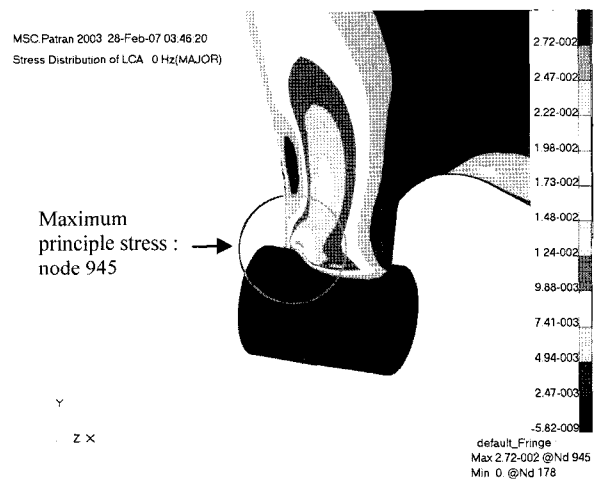


Figure 8. Stress distribution of the lower control arm when excited at 0 Hz (unit load).

the frequency response analysis at 0 Hz. When the maximum principal stress distribution from the frequency response analysis and the dynamic load profile were superimposed on the vibration fatigue analysis, the highest damage rate was $3.06 \times 10^{-8}$ at node 945. Table 4 lists the five nodes with the highest damage rate in descending

Table 4. Damage rate based on vibration fatigue analysis.

| Node | Damage rate (Damage/sec) | Life seconds |
|---|---|---|
| 945 | 3.06E-08 | 3.27E+07 |
| 11951 | 1.97E-09 | 5.07E+08 |
| 11952 | 1.90E-09 | 5.27E+08 |
| 881 | 1.70E-09 | 5.89E+08 |
| 853 | 1.62E-09 | 6.17E+08 |

order. Node 945 had more than 10 times the amount of damage as any other node. A reduction in the damage rate of the most susceptible node should be the target of an optimal design.

## 5. OPTIMAL SHAPE DESIGN

A durability analysis of the baseline model permitted us to select the control factors and their levels. Based on the sensitivity of each factor, which could be assessed using the design of the experimental approach, the optimal lower control arm shape could be obtained using the response surface method. The aim of this procedure in our study was to reduce the damage rate of node 945, which was found to have the highest damage rate in the preceding analysis, and the mass of the optimized model is not to exceed 105% of the mass of the baseline model.

$$\textit{Minimize damage rate of node 945}$$
$$\textit{Subject to Mass} \leq \textit{Mass\_initial} \times 1.05 \quad (9)$$

### 5.1. Selection of the Control Factors and Levels

The control factors for the shape optimization are shown in Figure 9. We focused on areas where the stress was concentrated and selected the following as control factors: the width and radius of four spots A, B, C, and D, and the thickness of upper shell E and lower shell F. Each factor was defined as having three levels. Each level was adjusted to be 10% greater or smaller than the baseline value.

### 5.2. Detection of Major Factors based on the Design of Experiment Approach

The design of experiment (DOE) approach was used to effectively identify the effect of the control factors (Phadke, 1989). Using this approach, the designer is able to determine the effect that each variable (factor) has on the outcome (target value) and calculate the variable value (level of factor) that meets the optimal conditions. The sequence of the general design of experiment approach is described in Figure 10.

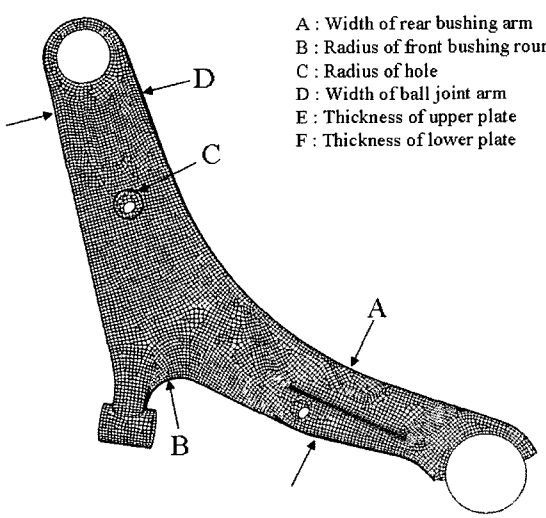


Figure 9. Control factors of lower control arm shape.

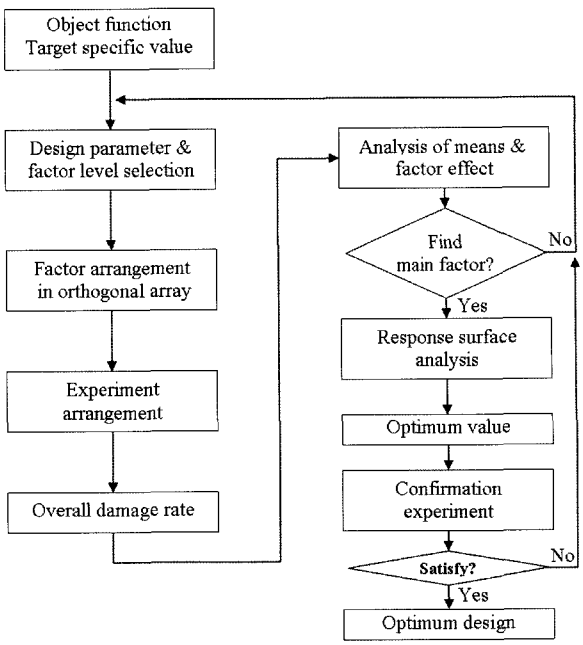


Figure 10. Optimal design process using the design of experiment approach.

An orthogonal array was used to perform an analysis of the means and examine factors that affected the target values. The analysis was performed with three levels for each of the six types of control factors using a proper $L_{27}(3^{13})$ orthogonal array. Shape of the lower control arm for each simulation was obtained by using HyperStudy, and fagitue analysis was performed by using MSC/FATIGUE respectively. Table 5 shows the orthogonal array and the results of the durability analysis at node 945 for different control factor levels. As was the case in the baseline model, the damage rate at node 945 was much higher than that at any other node. Table 6 lists the damage rates for three highest nodes for the cases with the highest and lowest total damage rates.

The effect of the factor level can be identified using the design of experiment approach based on the orthogonal array. The effect of the factor level is defined as the deviation between the average balanced by the factor level and the overall average balanced across the entire scope of the experiment. Figure 11 shows the main effect of each factor. The figure indicates that the control factors that were sensitive to specific values were the widths of the arm and the thicknesses of the upper and lower shell: factors A, D, E, and F. For the E and F factors, which were the thicknesses of the shell. The damage rate varied almost linearly with the change in the level, indicating

Table 5. Orthogonal array and damage rate by simulation.

| Run | A | B | C | D | E | F | DamageRate | Mass (kg) |
|---|---|---|---|---|---|---|---|---|
| 1 | 1 | 1 | 1 | 1 | 1 | 1 | 5.41E-08 | 3.27 |
| 2 | 1 | 1 | 2 | 2 | 2 | 2 | 1.59E-08 | 3.56 |
| 3 | 1 | 1 | 3 | 3 | 3 | 3 | 5.47E-09 | 3.84 |
| 4 | 1 | 2 | 1 | 2 | 3 | 3 | 6.74E-09 | 3.90 |
| 5 | 1 | 2 | 2 | 3 | 1 | 1 | 5.47E-08 | 3.26 |
| 6 | 1 | 2 | 3 | 1 | 2 | 2 | 1.49E-08 | 3.53 |
| 7 | 1 | 3 | 1 | 3 | 2 | 2 | 8.10E-09 | 3.59 |
| 8 | 1 | 3 | 2 | 1 | 3 | 3 | 7.01E-09 | 3.86 |
| 9 | 1 | 3 | 3 | 2 | 1 | 1 | 5.02E-08 | 3.24 |
| 10 | 2 | 1 | 1 | 3 | 3 | 2 | 7.54E-09 | 3.80 |
| 11 | 2 | 1 | 2 | 1 | 1 | 3 | 1.66E-08 | 3.55 |
| 12 | 2 | 1 | 3 | 2 | 2 | 1 | 2.34E-08 | 3.44 |
| 13 | 2 | 2 | 1 | 1 | 2 | 1 | 2.43E-08 | 3.48 |
| 14 | 2 | 2 | 2 | 2 | 3 | 2 | 4.47E-09 | 3.77 |
| 15 | 2 | 2 | 3 | 3 | 1 | 3 | 1.71E-08 | 3.54 |
| 16 | 2 | 3 | 1 | 2 | 1 | 3 | 4.62E-09 | 3.58 |
| 17 | 2 | 3 | 2 | 3 | 2 | 1 | 2.99E-08 | 3.47 |
| 18 | 2 | 3 | 3 | 1 | 3 | 2 | 9.31E-09 | 3.74 |
| 19 | 3 | 1 | 1 | 2 | 2 | 3 | 1.08E-08 | 3.80 |
| 20 | 3 | 1 | 2 | 3 | 3 | 1 | 1.11E-08 | 3.68 |
| 21 | 3 | 1 | 3 | 1 | 1 | 2 | 2.33E-08 | 3.44 |
| 22 | 3 | 2 | 1 | 3 | 1 | 2 | 2.87E-08 | 3.49 |
| 23 | 3 | 2 | 2 | 1 | 2 | 3 | 4.43E-09 | 3.77 |
| 24 | 3 | 2 | 3 | 2 | 3 | 1 | 1.16E-08 | 3.66 |
| 25 | 3 | 3 | 1 | 3 | 3 | 1 | 1.43E-08 | 3.71 |
| 26 | 3 | 3 | 2 | 1 | 1 | 2 | 2.73E-08 | 3.46 |
| 27 | 3 | 3 | 3 | 2 | 2 | 3 | 1.07E-08 | 3.75 |

Table 6. Simulation of the minimum and maximum damage rates and comparison.

| | | Base | Run #5 | Run #23 |
|---|---|---|---|---|
| Damage rate | Node 945 | 3.06E-08 | 5.47E-08 | 4.43E-09 |
| | Node 11951 | 1.97E-09 | 7.94E-09 | 9.28E-10 |
| | Node 11952 | 1.90E-09 | 7.98E-09 | 9.36E-10 |
| Mass (kg) | | 3.62 | 3.26 | 3.77 |

that the damage rate decreased as the upper and lower shell became thicker. Therefore, an improved lower control arm shape could be obtained if the A and D factors were chosen for a response surface analysis.

### 5.3. Response Surface Analysis

A response surface analysis is a statistical approach that analyzes the response surface when several variables combine to produce a complex effect on a certain response factor (Park, 2003). A regression analysis was performed

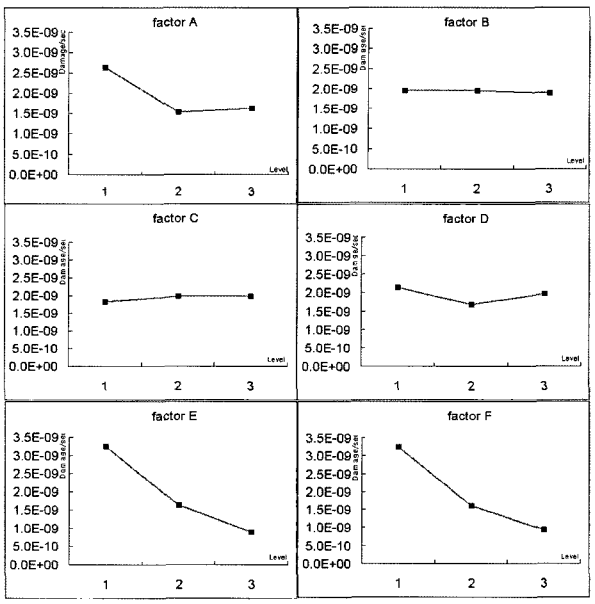


Figure 11. Plots of the factor effects.

to determine the damage rates of the lower control arm in the form of a function of the two control factors so that we could find the optimal shape that would enhance the durability life of the arm. A quadratic regression function obtained using a central composite design (CCD) can be expressed as

$$y = \beta_0 + \sum_{i=1}^{2} \beta_i x_i + \sum_{i=1}^{2} \beta_{ii} x_{ii} + \sum_{i<j}^{2} \beta_{ij} x_i x_j + e\,, \qquad (10)$$

where y, $\beta$, and $x_i$ are the response factor, regression coefficient, and control factor, respectively, and $e$ is the error term. The experimental points of the CCD used to adjust the second response surface included $2^k$ experimental points of the $2^k$ factor experiment, $2k$ axis points, and $n$ ($\geq$1) central point.

We analyzed a total of nine spots with one central spot as well as axis points of 1.414 and –1.414 on the two axes. Based on the design of experiment approach using an orthogonal array, the factors of A and D were linearly converted into $x_1$ and $x_2$ using

$$W(\%)=5+2.5x, \qquad (11)$$

where $W$ refers to factor A or factor D and $x$ is each linearized factor for the response surface analysis. However, considering the effect and cost of the overall system, the mass of the optimized model was set to not exceed 105% of the mass of the baseline model. For the same reason, the B, C, E, and F factors were fixed at levels 3, 1, 2, and 2, respectively. Also regression functions were obtained using MINITAB, which is a commercial statistics code. Table 7 gives the factor levels for the

Table 7. Results of the response surface analysis.

| Run | x1 | x2 | Damage Rate | Mass (kg) |
|---|---|---|---|---|
| 1 | −1 | −1 | 9.42E-09 | 3.77 |
| 2 | −1 | 1 | 6.06E-09 | 3.78 |
| 3 | 1 | −1 | 5.93E-09 | 3.82 |
| 4 | 1 | 1 | 5.18E-09 | 3.83 |
| 5 | 0 | 0 | 4.71E-09 | 3.80 |
| 6 | −1.414 | 0 | 8.58E-09 | 3.77 |
| 7 | 1.414 | 0 | 5.38E-09 | 3.83 |
| 8 | 0 | −1.414 | 5.41E-09 | 3.80 |
| 9 | 0 | 1.414 | 4.97E-09 | 3.83 |

response surface analysis and the corresponding results.

A quadratic regression function of the damage rate and mass based on the above results is

$$y_D = 4.7112\times10^{-9} - 1.1124\times10^{-9}x_1 - 5.9193\times10^{-10}x_2 + 1.2745\times10^{-9}x_1^2 + 3.7896\times10^{-10}x_2^2 + 6.5100\times10^{-10}x_1x_2 \quad (12)$$

$$y_{mass} = 3.082 + 0.0223x_1 + 0.0069x_2 - 0.0029x_1^2 + 0.0036x_2^2 - 0.0015x_1x_2 \quad (13)$$

Coefficient of determination, $R^2$ in regression fuctions in terms of damage rate and mass are 0.924, and 0.961 each. As a regression fuction could be determined to be appropriate when $R^2$ is lager than 0.7 (Park, 2003), it is also appropriate to approximate control factor as a quadratic response surface.

Eigenvalues obtained through a canonical analysis indicate that the optimal spot is the minimum point since the signs of eigenvalues $\lambda_1$=1.380×10$^{-9}$ and $\lambda_2$=2.732×10$^{-10}$ are positive. Values that minimize the damage rate can be determined using a contour plot.

Figure 12 shows a contour plot of the two converted factors $x_1$ and $x_2$. A plot created by pairing up the two factors indicated that the minimum damage rate, 4.39×10$^{-9}$, was obtained for a mass of 3.81 kg when the response factors $x_1$ and $x_2$ were 0.304 and 0.520, respectively. Therefore, the optimal model was obtained when the width of factors A and D were 5.76% and 6.30% thicker than the baseline model, which increased the mass of the lower control arm by 5.3%. Another test was performed to verify the optimal value obtained through the response surface analysis; these results are shown in Table 8. The damage rates calculated from the verification test and the response surface analysis agreed with each other to within 2.2%. The two masses were within 1.8%.

The optimal damage rate was 2% lower than the minimum damage rate when the design of experiment procedure was used. However, the damage rate can be reduced further if the levels of factors B, C, E, and F are changed to equivalent levels as the response surface analysis is performed.

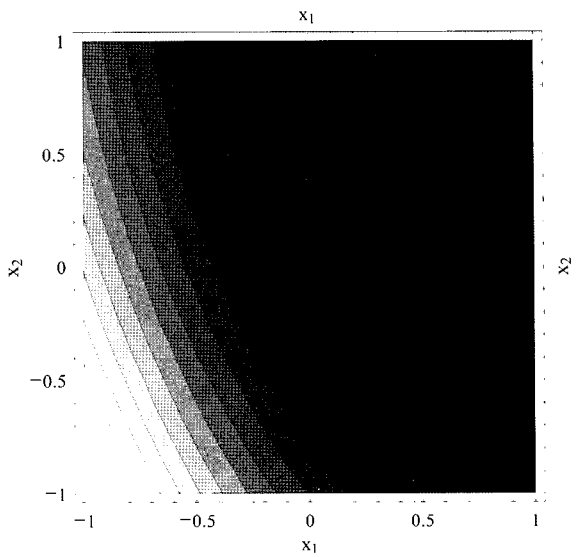


Figure 12. Contour plot of factors $x_1$ and $x_2$.

Table 8. Damage rate and mass of the optimized model.

| | Response surface analysis | Confirmation experiment | Error (%) |
|---|---|---|---|
| Damage rate (Node 945) | 4.39E-09 | 4.48E-09 | 2.02 |
| Mass (kg) | 3.81 | 3.75 | 1.80 |

## 6. CONCLUSIONS

This study evaluated the durability life of a lower control arm, which is a suspension component in a vehicle. The evaluation considered the dynamic effects of the arm. The analysis was performed using the design of experiment approach and a response surface analysis to increase the durability life of the arm. The following are the summary and our conclusions.

(1) We converted the dynamic load profile of the suspension system in the time domain obtained during a virtual driving test into a power spectral density and used a probability density function to evaluate the durability life while considering the dynamic characteristics of the system. We also conducted a frequency response analysis within the excitation range.

(2) We selected six control factors representing the lower control arm shape and applied an experimental sensitivity approach to analyze their relative importance. Each factor had three levels, and we performed a test using the $L_{27}3^{13}$ orthogonal array to identify its sensitivity.

(3) The most sensitive four factors were identified using the design of experiment approach. Based on this result, we obtained an improved lower control arm model using a response surface analysis. Using a central composite design, we selected nine experimental points to form the response surface and obtained a quadratic regression function for the mass and damage rate based on the outcome of the analysis. The optimal points that minimized the damage rate of the area of interest were identified using a regression function. The mass of the model increased with the level of the control factor and the change in the damage rate over the change in mass was relatively large. Therefore, when selecting experimental points for the response surface analysis, we adjusted the mass of the lower control arm to remain at a level similar to the mass of the baseline model.

(4) The response surface analysis showed that the minimum damage rates were achieved when the two response factors $x_1$ and $x_2$, had values of 0.304 and 0.520, respectively, yielding a damage rate of $4.39\times 10^{-9}$ and a mass of 3.81 kg. The differences between the damage rate and the mass obtained using the regression function and those obtained from a verification test were 2.02 and 1.80%, respectively, which are sufficiently small.

The study demonstrated that a systematic design approach could be used to enhance the durability performance of a vehicle by reducing the damage to the lower control arm and thus the front wheel suspension system. Such an approach would be valid for other cases that require a performance analysis that considers dynamic effects.

## REFERENCES


Bendat, J. S. (1964). Probability functions for random responses. *NASA Report on Contract*, NAS-5-4590.

Berzri, M., Dhir, A., Ranganathan, R., Balendran, B. and Jayakumar, P. (2004). A new tire model for road loads simulation: Full vehicle validation. *SAE Paper No.* 2004-01-1579.

Bishop, N. W. M. (1988). *The Use of Frequency Domain Parameters to Predict Structural Fatigue.* University of Warwick. Ph. D. Dissertation. Coventry. UK.

Bishop, N. W. M. and Sheratt, F. (1989). Fatigue life prediction from power spectral density data. *Environmental Engineering*, **2,** 11–19.

Bishop, N. W. M., Steinbeck, J. and Sherratt, F. (2000). *Finite Element Based Fatigue Calculations* (NAFEMS). Glasgow, UK.

Choi, B. L., Choi, J. H. and Choi, D. H. (2005). Reliability-based design optimization of an automotive suspension system for enhancing kinematic and compliance characteristics. *Int. J. Automotive Technology* **6, 3**, 235–242.

Choi, K. K., Youn, B. D., Tang, J. and Hardee, E. (2005). Reliability-based analysis and design optimization for durability. *Proc. SPIE-Int. Soc. Opt. Eng.* **5805, 1**, 74–84.

Dirlik, T. (1985). *Application of Computers in Fatigue Analysis*. University of Warwick. Ph. D. Dissertation. Coventry. UK.

Ghosh, S. and Medepalli, S. (2005). Effect of tire stiffness on vehicle loads. *SAE Paper No.* 2005-01-0825.

Haiba, M., Barton, D. C., Brooks, P. C. and Levesley, M. C. (2003). Using a quarter-vehicle multi-body model to estimate the service loads of a suspension arm for durability calculations. *Proc. Instn. Mech. Engrs. Part K: J. Muti-body Dynamics*, **217,** 121–133.

Heinrietz, A., Lehrke, H. P., Rupp, A. N. and Barthel, C. (2003). Identification of parametric tire models for the fatigue evaluation of suspension components. *SAE Paper No.* 2003-01-1276.

Jung, D. H. and Bae, S. I. (2005). Automotive component fatigue life estimation by frequency domain approach. *Key Engineering Materials* **297, 300**, 1776–1783.

Kim, G. H., Noh, K. H., Kim, D. S. and Ko, W. H. (2003). *Development of Reliability/Durability Evaluation for Vehicle and Components Applied by Virtual Testing Technology.* Body and Chassis Engineering Laboratory. KATECH. Korea.

Kim, H. S., Yim, H. J. and Kim, C. B. (2002). Computational durability prediction of body structures in prototype vehicles. *Int. J. Automotive Technology* **3, 4**, 129–135.

Lee, S. B., Han, W. S. and Yim, H. J. (2003). Fatigue analysis of automotive suspension system considering dynamic effect. *SAE Paper No.* 2003-01-2814.

Lee, Y. L., Pan, J., Hathaway, B. R. and Barkey, E. M. (2005). *Fatigue Testing and Analysis*. Elsevier. New York.

Mechanical Dynamics Inc. (1998). *MSC/ADAMS User Manual.* Irvine. CA. USA.

MSC Software Co. (2003). *MSC/FATIGUE Quick Start Guide*. Santa Ana. CA. USA.

MSC Software Co. (2002), *MSC/NASTRAN 2001 Reference Manual.* Santa Ana. CA. USA.

Park, S. H. (2003). *Design of Experiments*. Minyoung-Sa. Daejeon. Korea.

Phadke, M. S. (1989). *Quality Engineering Using Robust Design.* Prentice Hall. New Jersey.